Diabetic hyperglycemia reduces Ca^{2+} permeability of extrasynaptic AMPA receptors in AII amacrine cells

Áurea Castilho[1,2], Eirik Madsen[1], António F. Ambrósio[2, 3, 4], Margaret L. Veruki[1] and Espen Hartveit[1]

[1]Department of Biomedicine, University of Bergen, Bergen, Norway.

[2]Institute of Biomedical Imaging and Life Sciences (IBILI), Faculty of Medicine, University of Coimbra, Coimbra, Portugal.

[3]Center for Neuroscience and Cell Biology. Institute of Biomedical Imaging and Life Sciences (CNC.IBILI) Consortium, University of Coimbra, Coimbra, Portugal.

[4]Association for Innovation and Biomedical Research on Light and Image, Coimbra, Portugal.

Running head: Diabetes changes extrasynaptic AMPARs in AII amacrines

Address for correspondence: Espen Hartveit, University of Bergen, Department of Biomedicine, Jonas Lies vei 91, N-5009 Bergen, Norway.

espen.hartveit@biomed.uib.no

Phone: +47-55586350

Fax: +47-55586360

Number of figures: 4

Number of tables: 0

ABSTRACT

There is increasing evidence that diabetic retinopathy is a primary neuropathological disorder that precedes the microvascular pathology associated with later stages of the disease. Recently, we found evidence for altered functional properties of synaptic AMPA receptors in A17, but not AII amacrine cells in the mammalian retina and the observed changes were consistent with an upregulation of the GluA2 subunit, a key determinant of functional properties of AMPA receptors, including Ca^{2+} permeability and *I-V* rectification properties. Here, we have investigated functional changes of extrasynaptic AMPA receptors in AII amacrine cells evoked by diabetes. With patch-clamp recording of nucleated patches from retinal slices, we measured Ca^{2+} permeability and *I-V* rectification in rats with ~3 weeks of streptozotocin-induced diabetes and age-matched, non-injected controls. Under bi-ionic conditions ($[Ca^{2+}]_{out}$=30 mM, $[Cs^{+}]_{in}$=171 mM), the reversal potential of AMPA-evoked currents indicated a significant reduction of Ca^{2+} permeability in diabetic animals (E_{rev}=-17.7 mV, P_{Ca}/P_{Cs}=1.39) compared to normal animals (E_{rev}=-7.7 mV, P_{Ca}/P_{Cs}=2.35). Insulin treatment prevented the reduction of Ca^{2+} permeability. *I-V* rectification was examined by calculating a rectification index (RI) as the ratio of the AMPA-evoked conductance at +40 and -60 mV. The degree of inward rectification in patches from diabetic animals (RI=0.48) was significantly reduced compared to that in normal animals (RI=0.30). These results suggest that diabetes evokes a change in the functional properties of extrasynaptic AMPA receptors of AII amacrine cells. These changes could be representative for extrasynaptic AMPA receptors elsewhere in AII amacrine cells and suggest that synaptic and extrasynaptic AMPA receptors are differentially regulated.

Key words: amacrine cells; calcium-permeable AMPA receptors; diabetes; retina

INTRODUCTION

Diabetic retinopathy is both the most common cause of legal blindness in working-age adults (reviewed by Gardner et al. 2011) and one of the most common complications of diabetes mellitus (henceforth referred to as diabetes). Although traditionally considered a microvascular disease, there is increasing evidence that diabetic retinopathy partially involves a dysfunction of the neural retina that precedes the microvascular pathology typically observed at later stages of the disease (Antonetti et al. 2012; Simó and Hernández 2014). Supporting the hypothesis that pre-vascular diabetic retinopathy could be a primary neuropathological disorder, is the accumulating evidence for diabetes-evoked changes in the functional state of specific neurotransmitter systems, with changes in expression and regulation of AMPA receptor subunits being subject to detailed investigations (Castilho et al. 2012; Gowda et al. 2011; Ng et al. 2004; Santiago et al. 2006, 2008; Semkova et al. 2010). Of particular interest is the GluA2 subunit, which plays a crucial role in determining important functional properties of AMPA receptors such as Ca^{2+} permeability, current-voltage (*I-V*) rectification, single-channel conductance, and kinetics (reviewed by Cull-Candy et al. 2006; Greger and Esteban 2007; Traynelis et al. 2010). Exposing retinal cultures enriched in amacrine cells to elevated glucose concentration induces a reduction in agonist-evoked Ca^{2+} responses mediated by Ca^{2+}-permeable AMPA receptors, most likely caused by a concomitant increase in the expression of the GluA2 subunit (Santiago et al. 2006). It is difficult to directly measure the Ca^{2+} permeability of AMPA receptors in intact systems, however, and changes in this important functional property is typically inferred indirectly by measuring changes in subunit expression or correlated changes in electrophysiological properties.

Recently, we used an experimental model of diabetes in mature rats to study synaptic transmission in the rod bipolar microcircuit and examined how diabetes differentially affects the functional properties of synaptic AMPA receptors expressed by AII and A17 amacrine cells, two important and well-characterized types of rod amacrine

cells in the mammalian retina (Castilho et al. 2015). The AII and A17 amacrine cells are postsynaptic to glutamatergic rod bipolar cells at dyad synapses (Kolb and Famiglietti 1974; Raviola and Dacheux 1987) and there is evidence that Ca^{2+}-permeable AMPA receptors are involved in mediating synaptic input from rod bipolar cells to both types of amacrine cells (Chávez et al. 2006; Osswald et al. 2007; Singer and Diamond 2003). Whereas the A17 amacrine cell provides a GABAergic reciprocal inhibitory synapse back onto the rod bipolar cell (Nelson and Kolb 1985; Raviola and Dacheux 1987), the AII amacrine cell outputs its signal to ON-cone bipolar cells via electrical synapses (Kolb and Famiglietti 1974; McGuire et al. 1984; Strettoi et al. 1992, 1994) and to OFF-cone bipolar cells via inhibitory, glycinergic synapses (Pourcho and Goebel 1985; Sassoè-Pognetto et al. 1994; Strettoi et al. 1992, 1994). In addition to the glutamatergic input from rod bipolar cells at the arboreal dendrites, AII amacrine cells also receive glutamatergic input from some types of OFF-cone bipolar cells at the lobular appendages (Kolb and Famiglietti 1974; Strettoi et al. 1992; Veruki et al. 2003). The main result of our recent study was that diabetes evoked changes in the functional properties of synaptic AMPA receptors of A17 amacrine cells, including reduced Ca^{2+} responses mediated by Ca^{2+}-permeable AMPA receptors, and the observed changes were consistent with an upregulation of the GluA2 subunit (Castilho et al. 2015). We did not find evidence for similar changes of synaptic AMPA receptors in AII amacrine cells.

There is evidence, however, that AII amacrine cells express extrasynaptic AMPA receptors with relatively high Ca^{2+} permeability at their somata (Mørkve et al. 2002), leaving open the possibility that diabetes might change extrasynaptic AMPA receptors on these cells which would not have been detected in our previous study of synaptic receptors. On this basis, we decided to investigate whether experimentally induced diabetes alters functional properties of somatic extrasynaptic AMPA receptors of AII amacrine cells. We were particularly interested in potential changes of Ca^{2+} permeability, which is of particular importance for neuronal signaling and plasticity (Higley and

Sabatini 2012). We recorded from nucleated patches isolated from AII amacrine cells and measured the relative Ca^{2+} permeability (under bi-ionic conditions) and the *I-V* rectification properties of the AMPA receptors. Here, we find that diabetes reduces both Ca^{2+} permeability and *I-V* inward rectification of extrasynaptic AMPA receptors in AII amacrine cells, suggesting that diabetes differentially regulates synaptic and extrasynaptic AMPA receptors in these cells.

METHODS

Retinal slice preparation. General aspects of the methods have previously been described in detail (Hartveit 1996; Mørkve et al. 2002). Female albino rats (Wistar HanTac; 5 - 8 weeks postnatal) were deeply anaesthetized with isoflurane in oxygen and killed by cervical dislocation (procedure approved under the surveillance of the Norwegian Animal Research Authority). Vertical retinal slices were visualized (Axioskop 2 FS, Zeiss) with a ×40 water immersion objective (0.9 NA; Olympus) and infrared differential interference contrast (IR-DIC) videomicroscopy. Recordings were carried out at room temperature (22 - 25°C).

Solutions and drug application. The standard extracellular perfusing solution was continuously bubbled with 95% O_2 - 5% CO_2 and had the following composition (in mM): 125 NaCl, 25 $NaHCO_3$, 2.5 KCl, 2.5 $CaCl_2$, 1 $MgCl_2$, 10 glucose, pH 7.4. In recordings designed to measure the relative Ca^{2+} permeability of AMPA receptor channels, recording pipettes were filled with an intracellular solution of the following composition (in mM): 150 CsCl, 5 Hepes, 2 MgATP and 10 EGTA. The pH was adjusted to 7.3 with CsOH, increasing the total Cs^+ concentration to 171 mM. The osmolality of this intracellular solution was ~290 mOsm/kg. In recordings designed to measure the *I-V* rectification properties, the pipettes were filled with an intracellular solution of the following composition (in mM): 125 $CsCH_3SO_3$, 15 TEA-Cl, 8 NaCl, 10 Hepes, 1 $CaCl_2$, 4 MgATP and

5 EGTA. Spermine (Research Biochemicals International, Natick, MA, USA) was added at a concentration of 100 μM, Lucifer yellow (Sigma-Aldrich) was added at a concentration of 1 mg/ml and pH was adjusted to 7.3 with CsOH. The osmolality of this intracellular solution was ~315 mOsm/kg. The data acquisition software (PatchMaster; HEKA Elektronik, Lambrecht/Pfalz, Germany) corrected all holding potentials for liquid junction potentials on-line. Theoretical liquid junction potentials were calculated with JPCalcW (Axon Instruments, Union City, CA, USA).

In experiments for measuring Ca^{2+} permeability of AMPA receptor channels in nucleated patches, S-AMPA (termed "AMPA" for simplicity; 1.6 mM; Tocris Bioscience, Bristol, UK) was applied from a theta-tube application pipette (nominal septum thickness ~117 μm; final tip diameter 250 - 300 μm; Hilgenberg, Malsfeld, Germany). The pipette tip with the nucleated patch was positioned near the interface between control solution and agonist-containing solution continuously flowing out of each barrel, about 100 μm downstream from the tip of the application pipette. The solution flow rate (5 ml/h) was maintained by syringe pumps (KDS220; KD Scientific, Boston, MA, USA) controlled by the PatchMaster software. Concentration jumps of agonist to a nucleated patch were applied by rapidly moving the position of the application pipette and thus the solution interface while the recording pipette remained still. Agonist pulses were applied every 4 s. The application pipette was mounted on a piezo actuator (LSS-3100/PZS-100HS; Burleigh Instruments, Fishers, NY, USA) operated by an amplifier (PZ-150M; Burleigh Instruments) stimulated with square-wave voltage pulses from the ITC-16 interface built into the recording amplifier (see below). Before being fed to the amplifier, the voltage pulses were smoothened by an electronic circuit consisting of an RC-filter (time constant 1 ms) and an inductive element to counteract oscillations. The 10 - 90% solution exchange time (~250 - 300 μs) was measured as the change in liquid junction current of an open patch pipette filled with 0.9% NaCl when moved from a solution of 0.9% NaCl to a solution of 0.09% NaCl. However, for a nucleated patch the measured exchange time represents an

underestimation of the true exchange time. To establish bi-ionic conditions during measurements of Ca^{2+} permeability, the nucleated patches were exposed to an extracellular solution containing (mM) 30 $CaCl_2$, 100 N-methyl-D-glucamine (NMDG), 10 Hepes and 25 glucose (pH adjusted to 7.4 with HCl). AMPA was dissolved in the same solution. For measurements of Ca^{2+} permeability, the reference electrode (Ag-AgCl wire) was connected to the recording chamber via an electrolyte-agar bridge to avoid directly exposing the reference electrode to changes of the extracellular solution.

Electrophysiological recording and data acquisition. Patch pipettes were pulled from thick-walled borosilicate glass (outer diameter, 1.5 mm; inner diameter, 0.86 mm). The open-tip resistance of the pipettes ranged from 5 to 7 MΩ when filled with intracellular solution. Voltage-clamp recordings were performed with an EPC9-dual amplifier (HEKA Elektronik) controlled by PatchMaster software. After establishing a GΩ-seal (initial seal resistance 2 - 25 GΩ), currents caused by the recording electrode capacitance (C_{fast}) were automatically measured and neutralized by the amplifier. After breaking into the cell, currents caused by the cell membrane capacitance (C_{slow}) were partially neutralized by the amplifier. To establish a nucleated patch recording, the pipette was slowly withdrawn after establishing the whole-cell recording configuration, while continuous light suction (~50 mbar) was applied to the pipette. When a nucleated patch was successfully isolated, the reduced membrane capacitance resulted in capacitative current transients of the opposite polarity that were cancelled by re-adjustment of the C_{slow} neutralization circuitry. The sampling interval was set to 50 μs and before sampling, signals were low-pass filtered (analog 3- and 4-pole Bessel filters in series) with a corner frequency (-3 dB) of 4 kHz.

Experimental model of type 1 diabetes. As in our previous study (Castilho et al. 2015), diabetes was induced in 4-week old rats with a single intraperitoneal injection of streptozotocin (65 mg/kg body weight), a toxin that kills β cells of the pancreatic islets of

Langerhans (Lenzen 2008). Animals used for control experiments did not receive any injections. Streptozotocin was stored at -20°C until the day of injection when it was dissolved in 10 mM Na-citrate buffer (pH 4.5). After injection, each rat was returned to its home cage and tested for development of diabetes by measuring the blood glucose concentration two days later. Blood glucose was measured with a hand-held glucometer (Contour Glucometer, Bayer) by collecting a drop of blood from the tail. The highest concentration we could measure with our glucometer was 600 mg/dl. Rats with blood glucose concentration exceeding 250 mg/dl were considered diabetic. At the day of the experiment diabetes was again verified by measuring blood glucose. Animals with diabetes were used for electrophysiological experiments 22 ± 0.8 days (range 18 - 26 days) after injection with streptozotocin. At the time of the experiments, the diabetic animals were between 6 and 8 weeks of age and the control animals were between 5 and 7 weeks of age. All animals were kept on a 12/12 light/dark cycle with free access to food and water.

When rats received treatment with insulin (Sigma-Aldrich), diabetes was first verified by measuring blood glucose two days after streptozotocin injection and then insulin was administered subcutaneously twice every day until the day of the experiment. During the first two days of insulin treatment, glucose concentration was measured twice daily and the dose of insulin was adjusted between 2-7 units to maintain the blood glucose concentration lower than 250 mg/dl. After the third day of insulin treatment, we found that administration of 6 units of insulin twice each day resulted in adequate glucose levels and this treatment continued without further adjustments until the day of the experiment. During this period, blood glucose concentration was measured once daily, before the second injection of insulin.

General data analysis. Data were analyzed with FitMaster (HEKA Elektronik), IGOR Pro (WaveMetrics, Lake Oswego, OR, USA), AxoGraph X (AxoGraph Scientific, Sydney,

188 Australia), Excel (Microsoft, Redmond, WA, USA) and GraphPad Prism (GraphPad
189 Software, La Jolla, CA, USA). The peak amplitude of AMPA-evoked currents was
190 measured as the mean amplitude between two vertical cursors positioned close to the
191 peak current response as identified by eye. Data points of *I-V* relationships were fitted by
192 third- to sixth-order polynomial functions. The order of the polynomial function was kept
193 as low as possible while still getting a good fit as determined by eye. Reversal potentials
194 (E_{rev}s) were determined by the intersection of the fitted line with the abscissa. As a
195 verification, we also measured the E_{rev}s by fitting a line to the two data points closest to the
196 presumed E_{rev} (i.e. the lowest amplitude inward and outward currents). The results were
197 very similar to those obtained by fitting all data points with polynomial functions. To
198 quantify the degree of rectification of *I-V* relationships, we used the following equation to
199 calculate a rectification index (RI) that expresses the ratio of chord conductance at +40 mV
200 and -60 mV ($RI = G_{+40} / G_{-60}$):

201 $$RI = \frac{I_{+40} / (40 - E_{rev})}{I_{-60} / (-60 - E_{rev})}, \quad (1)$$

202 where I_{+40} and I_{-60} are the currents at +40 mV and -60 mV, respectively, and E_{rev} is the
203 reversal potential in mV. Data are presented as means ± SEM (n = number of cells).
204 Statistical analysis with comparisons between two groups (normal, diabetes) were
205 performed using Student's two-tailed t test (unpaired) and comparisons between three
206 groups (normal, diabetes, insulin-treated diabetes) were performed using analysis of
207 variance (ANOVA) followed by Tukey's multiple comparison procedure to obtain
208 adjusted P-values. Differences were considered statistically significant at the $P < 0.05$ level.
209 The number of individual traces included in the averaged traces in the figures is stated for
210 each case. For illustration purposes, most raw data records were low-pass filtered (digital
211 nonlagging Gaussian filter, -3 dB at 500 Hz – 2 kHz).
212

Determination of Ca^{2+} permeability. To determine the relative Ca^{2+} permeability, bi-ionic conditions were established by recording with an intracellular solution containing Cs^+ (nominally 171 mM) as the only permeant cation and an extracellular solution containing Ca^{2+} (nominally 30 mM) as the only permeant cation. Monovalent cations (Na^+ and K^+) were substituted with $NMDG^+$ because AMPA receptors are not measurably permeable to this cation (Iino et al. 1990; Jonas and Sakmann 1992). E_{rev} was determined from currents evoked by application of AMPA at a series of holding potentials. The relative permeability of Ca^{2+} compared with Cs^+ (P_{Ca}/P_{Cs}) was subsequently calculated from the following equation derived from the Goldman-Hodgkin-Katz constant-field equation (Iino et al. 1990):

$$\frac{P_{Ca}}{P_{Cs}} = \frac{\left[Cs^+\right]_{in}}{\left[Ca^{2+}\right]_{out}} \times \frac{\exp\left(E_{rev}F/RT\right)\left[\exp(E_{rev}F/RT)+1\right]}{4}, \qquad (2)$$

where F is Faraday's constant, R is the universal gas constant, T is the absolute temperature, and P_{Ca} and P_{Cs} represent the permeability coefficients of Ca^{2+} and Cs^+, respectively. Other ions are not taken into account and it is assumed that $[Ca^{2+}]_{in}$ and $[Cs^+]_{out}$ are zero. The concentrations were corrected by multiplying by activity coefficients (0.551 for Ca^{2+} and 0.707 for Cs^+; see Mørkve et al. 2002 for details).

Fig. 1 near here

RESULTS

Identification of AII amacrine cells in retinal slices and isolation of nucleated patches. In recordings designed to estimate the relative Ca^{2+} permeability of AMPA receptors in nucleated patches from AII amacrine cells, it was not possible to verify the identity of the recorded cells with fluorescence microscopy because the requirement for bi-ionic

conditions excluded the addition of Lucifer yellow to the intracellular solution. Considerable care was therefore taken to target cells that displayed the complete morphological characteristics of AII amacrines, as judged by the appearance of retinal slices imaged with IR-DIC videomicroscopy (Fig. 1*A*). Specifically, the criteria were the location of the cell body at the border of the inner nuclear layer and the inner plexiform layer and the presence of a thick apical dendrite descending into the inner plexiform layer. In addition, immediately following the establishment of the whole-cell configuration, we verified that 5 mV depolarizing test pulses (5 ms duration) from a holding potential of -60 mV evoked the characteristic inward action currents corresponding to unclamped action potentials (Fig. 1*B*) that depend on TTX-sensitive voltage-gated Na^+ channels (Mørkve et al. 2002; Veruki et al. 2003). In previous studies, we have found that all cells visually targeted by the above criteria that also subsequently display the characteristic action currents, can be positively identified as AII amacrine cells when examined with fluorescence microscopy (Mørkve et al. 2002; Veruki et al. 2003). Only cells that satisfied these selection criteria have been included in the material reported here. In recordings from nucleated patches where the goal was to study *I-V* rectification properties, Lucifer yellow was added to the intracellular solution and fluorescence microscopy could be used to verify the identity of the cells we recorded from.

For our study, we used a total of 9 normal, 8 diabetic, and 3 insulin-treated rats. For the rats injected with streptozotocin, the blood glucose concentration ranged from 290 to ≥600 mg/dl two days after injection and from 537 to ≥600 mg/dl at the day of the experiment. Before injection, the blood glucose in these rats was 89 ± 3 mg/dl (range 76 - 101 mg/dl), similar to the concentration measured in four normal controls tested at the day of the experiment (82 ± 6 mg/dl; range 67 - 94 mg/dl).

AMPA-evoked currents in nucleated patches. Nucleated patches (Fig. 1C) voltage-clamped at -60 mV were transiently exposed to AMPA (1.6 mM) using a theta-tube fast-

application system. In all cases, the nucleated patches responded with an inward current that rose to a peak followed by an exponential decay to a much smaller steady-state level during sustained agonist application (Fig. 1*D*), corresponding to rapid and strong desensitization (Mørkve et al. 2002; Veruki et al. 2003). Previous work indicates that the receptors mediating the response to AMPA are high-affinity AMPA / low-affinity kainate receptors, as opposed to high-affinity kainate / low-affinity AMPA receptors (Mørkve et al. 2002).

Fig. 2 near here

Ca^{2+} permeability of AMPA receptor channels in nucleated patches from normal and diabetic rats. To study the selectivity of the AMPA receptor channels for Ca^{2+} ions, we recorded agonist-evoked responses in nucleated patches under bi-ionic conditions with nominal concentrations of 171 mM Cs^+ intracellularly and 30 mM Ca^{2+} extracellularly (see METHODS). Figure 2, *A* and *B*, shows an example of responses evoked by AMPA (1.6 mM) at a series of holding potentials together with the corresponding *I-V* curve for the peak response (E_{rev} = -4.0 mV). Because the steady-state response component in some patches was too small for accurate measurement, it was not used for analysis. The average E_{rev} for nucleated patches isolated from normal animals was -7.7 ± 0.9 mV (Fig. 2*E*; range -11.3 to -4.0 mV; n = 7 patches). From these values, the permeability ratio (P_{Ca}/P_{Cs}) of the AMPA receptors expressed in the cell bodies of AII amacrines was calculated according to eqn (2), yielding an average value of 2.35 ± 0.11 (range 1.92 – 2.89). These results are very similar to those reported in the earlier study by Mørkve et al. (2002; E_{rev} = -10.7 ± 1.8 mV; P_{Ca}/P_{Cs} = 2.1 ± 0.21).

Nucleated patches isolated from AII amacrine cells from diabetic animals were investigated identically to nucleated patches from normal animals. Figure 2, *C* and *D*, shows an example of responses evoked by AMPA (1.6 mM) at a series of holding

potentials, together with the corresponding *I-V* relationship (E_{rev} = -13.7 mV). The average E_{rev} for AMPA-evoked responses in nucleated patches isolated from diabetic rats was -17.7 ± 1.8 mV (Fig. 2*E*; range -32.4 to -13.1 mV; n = 11 patches). The corresponding permeability ratio (P_{Ca}/P_{Cs}) was 1.39 ± 0.1 (range 0.65 – 1.74), significantly lower than the corresponding ratio in patches from normal rats (Fig. 3*C*; $F_{(2,20)} = 25.12$, $P < 0.0001$, one-way ANOVA followed by Tukey's post-hoc test). This change corresponds to a reduction in the Ca^{2+} permeability of the AMPA receptor channels of AII amacrine cells in diabetic animals and suggests a change in the subunit composition of the AMPA receptors.

Fig. 3 near here

Insulin treatment of diabetic rats prevents the reduced Ca^{2+} permeability of AMPA receptor channels in nucleated patches. If hyperglycemia is causally related to the reduced Ca^{2+} permeability observed in nucleated patches from AII amacrines in diabetic rats, it should be possible to prevent the reduction by maintaining normoglycemia with insulin treatment. To investigate this, we injected 4-week old rats with streptozotocin in the same way as described earlier, verified the development of hyperglycemia two days after injection and then started treatment with insulin. After a period of 15 - 17 days with insulin treatment, nucleated patches were isolated from AII amacrines and tested with application of AMPA in the same way as described above. Figure 3, *A* and *B*, shows an example of responses evoked by AMPA at a series of holding potentials, together with the corresponding *I-V* relationship (E_{rev} = -8.8 mV). The average E_{rev} for AMPA-evoked responses in nucleated patches isolated from diabetic rats treated with insulin was -9.1 ± 0.5 mV (Fig. 2*E*; range -10.9 to -8.2 mV; n = 5 patches). The corresponding permeability ratio (P_{Ca}/P_{Cs}) was 2.17 ± 0.06 (range 1.96 – 2.28), significantly different from diabetic rats that were not treated with insulin (Fig. 3*C*; $F_{(2,20)} = 25.12$, $P = 0.0003$, one-way ANOVA followed by Tukey's post-hoc test), but not significantly different from normal animals

($F_{(2,20)}$ = 25.12, P = 0.567, one-way ANOVA followed by Tukey's post-hoc test). This indicated that insulin treatment was able to prevent the diabetes-evoked reduction in the Ca^{2+} permeability of the AMPA receptors of AII amacrine cells, suggesting that the associated hyperglycemia could be causally involved.

Fig. 4 near here

Current-voltage relationships of AMPA-evoked currents in Na^+-rich external solution. The subunit composition of an AMPA receptor determines not only Ca^{2+} permeability, but also other functional properties like single-channel conductance, kinetics and current-voltage rectification (for review see Greger and Esteban 2007). To investigate the rectification properties of AMPA receptors in AII amacrine cells, we used a Na^+-rich external solution. Because intracellular polyamines are important for the rectification properties of certain types of non-NMDA receptor channel (Kamboj et al. 1995; Koh et al. 1995), we added spermine (100 μM) to the pipette solution to prevent washout of intracellular polyamines from being a confounding factor. Figure 4*A* shows an example of nucleated patch responses evoked by AMPA (1.6 mM) at a series of holding potentials, with the patch taken from a normal animal. The corresponding *I-V* relationship for the peak response displays clear inward rectification (Fig. 4*B*). We calculated the RI as the ratio between the chord conductances at +40 mV and -60 mV according to eqn (1). For the nucleated patch illustrated in Fig. 4, *A* and *B*, we found E_{rev} = -1.7 mV and RI = 0.27. For all nucleated patches from normal animals, the average values were 0.51 ± 2.70 mV (range -11.8 – 12.6 mV) for E_{rev} and 0.30 ± 0.02 (range 0.23 – 0.44) for RI (n = 9 patches; Fig. 4*E*). Next, we performed similar experiments with diabetic animals (2 - 3 weeks after the induction of diabetes). Figure 4*C* shows an example of nucleated patch responses evoked by AMPA (1.6 mM) at a series of holding potentials, with the patch taken from a diabetic animal. The corresponding *I-V* relationship for the peak response displays inward rectification (Fig.

4*D*). For this patch, we found E_{rev} = 6.4 mV and RI = 0.39. For all nucleated patches from diabetic animals, the average values were 7.7 ± 3.9 mV (range -8.4 – 29.2 mV) for E_{rev} and 0.48 ± 0.07 (range 0.27 – 0.89) for RI (n = 10 patches; Fig. 4*E*). The average RI was significantly higher than that from normal rats (P = 0.04; unpaired t test), reflecting a measurable decrease in inward rectification.

DISCUSSION

Here we have studied the effect of diabetes on functional properties of extrasynaptic AMPA-type glutamate receptors on the cell bodies of AII amacrine cells in the rat retina. Specifically, we used electrophysiological recording from nucleated patches to measure the relative Ca^{2+} permeability and *I-V* rectification of these receptors. Our major finding is that diabetes evokes both a decrease in Ca^{2+} permeability and a decrease in inward rectification of the *I-V* relationship. The most parsimonious interpretation of these results is that diabetes leads to a change in the subunit composition of the somatic extrasynaptic AMPA receptors of AII amacrine cells, most likely corresponding to an upregulation and increased content of the GluA2 subunit. These results raise a series of questions with respect to the relation between synaptic and extrasynaptic AMPA receptors of AII amacrine cells, how each might be influenced by diabetes and what the functional consequences of such changes could be.

Functional properties of synaptic and extrasynaptic AMPA receptors expressed by AII amacrine cells. Morphological investigations have not demonstrated synaptic input from rod or cone bipolar cells to the cell bodies of AII amacrine cells (e.g. Strettoi et al. 1992). Nevertheless, electrophysiological recordings from nucleated patches of AII amacrine cells have demonstrated the presence of non-NMDA-type ionotropic glutamate receptors with relatively high Ca^{2+} permeability and moderate inward rectification, and pharmacological analysis indicated the expression of AMPA, but not kainate receptors (Mørkve et al. 2002).

374 Furthermore, ultrafast application of glutamate to somatic outside-out patches from AII
375 amacrine cells evokes strongly desensitizing responses with very fast deactivation and
376 desensitization kinetics (Veruki et al. 2003). These results suggest the expression of AMPA
377 receptors with relatively low levels of the GluA2 subunit. The receptors examined in
378 somatic patches are most definitely extrasynaptic receptors, raising the question of how
379 similar they are to the synaptic receptors which mediate input from rod bipolar cells at the
380 arboreal dendrites and OFF-cone bipolar cells at the lobular appendages. Both the kinetic
381 and pharmacological properties of synaptic non-NMDA receptors, as studied by
382 electrophysiological recording of spontaneous excitatory postsynaptic currents (spEPSCs),
383 suggest a strong degree of similarity with the somatic extrasynaptic receptors (Veruki et al.
384 2003), but there is less direct evidence for high Ca^{2+} permeability of the synaptic AMPA
385 receptors of AII amacrine cells. First, paired recordings of synaptically coupled rod bipolar
386 cells and AII amacrine cells indicate moderate inward *I-V* rectification, suggesting
387 expression of Ca^{2+}-permeable receptors (Singer and Diamond 2003). Second, stimulation
388 with kainate evokes influx of Co^{2+} through Ca^{2+}-permeable AMPA receptors and the
389 pattern of Co^{2+} accumulation suggests that the relevant receptors are located not only at
390 the cell bodies of AII amacrines, but at dendritic processes as well (Osswald et al. 2007).
391 Finally, immunocytochemical investigations have found evidence for the presence of
392 GluA4 (and GluA3), but not GluA2, in synapses between rod bipolar cells and AII
393 amacrine cells (Ghosh et al. 2001; Li et al. 2002; Qin and Pourcho 1999). To our knowledge,
394 there are no published reports of corresponding functional and morphological data for the
395 synapses between OFF-cone bipolar cells and AII amacrine cells. Taken together, these
396 results suggest a high degree of similarity between the functional properties of
397 extrasynaptic somatic AMPA receptors and synaptic AMPA receptors in AII amacrine
398 cells. It is unknown, however, if the functional properties of the somatic AMPA receptors
399 correspond to the functional properties of putative extrasynaptic AMPA receptors located
400 at AII processes close to the synaptic inputs of rod bipolar and/or OFF-cone bipolar cells.

401

402 *Diabetes-evoked changes of AMPA receptors of AII amacrine cells.* We recently found
403 evidence for diabetes-evoked changes of the functional properties of synaptic AMPA
404 receptors in A17, but not AII amacrine cells in rat retina (Castilho et al. 2015). The changes
405 were observed by electrophysiological recording of spEPSCs and corresponded to a
406 reduction in the single-channel conductance and altered pharmacological properties,
407 consistent with an upregulation of the GluA2 subunit and reduced Ca^{2+} permeability. In
408 addition, two-photon imaging revealed reduced agonist-evoked influx of Ca^{2+} in the
409 dendritic varicosities of A17 amacrine cells from diabetic animals. There are at least three
410 ways the results of the present study can be interpreted in light of the lack of any diabetes-
411 evoked functional changes of synaptic AMPA receptors of AII amacrines reported in our
412 recent study (Castilho et al. 2015). First, it is possible that the changes we have observed
413 for somatic extrasynaptic AMPA receptors are predictive of similar changes occuring for
414 extrasynaptic AMPA receptors located elsewhere in AII amacrine cells. This could mean
415 that diabetes reduces the Ca^{2+} permeability not only of somatic, but also of putative
416 dendritic extrasynaptic AMPA receptors. This possibility cannot be eliminated because
417 changes of dendritic extrasynaptic receptors would not have been detected in our previous
418 study with recording of spEPSCs. Second, despite the fact that we did not detect any
419 physiological, pharmacological or biophysical differences between spEPSCs in AII
420 amacrines of normal and diabetic animals (Castilho et al. 2015), it is not possible to exclude
421 the possibility that diabetes could reduce the Ca^{2+} permeability of synaptic AMPA
422 receptors in these cells, independent of any potential changes of dendritic extrasynaptic
423 AMPA receptors. On the basis of established properties of Ca^{2+}-permeable AMPA
424 receptors (Cull-Candy et al. 2006), it is unlikely that a change in Ca^{2+} permeability would
425 occur without concomitant changes in other functional properties, but without being able
426 to directly measure the Ca^{2+} permeability of the synaptic AMPA receptors, the possibility
427 cannot be excluded. A complicating factor is that Ca^{2+}-permeable AMPA receptors can be

involved in mediating synaptic input from both OFF-cone bipolar cells at the lobular dendrites and from rod bipolar cells at the arboreal dendrites of AII amacrines, and receptors at the different synapses could be differentially regulated. If diabetes reduces the Ca^{2+} permeability at either location of synaptic AMPA receptor by changing the receptor subunit composition, the change was not detected by our physiological, pharmacological and biophysical analysis. Although unlikely, it is difficult to completely rule out the possibility of a change in subunit composition that leads to a dissociation between Ca^{2+} permeability and other physiological, pharmacological and biophysical properties. There is some evidence that these functional properties of AMPA receptors are not as closely correlated as originally believed, such that determination of one property does not necessitate expression of the other (reviewed by Bowie 2012). The third interpretation of the present results is that the synaptic and extrasynaptic (somatic) AMPA receptors of AII amacrine cells are genuinely different, either with respect to their subunit composition, their posttranslational modification or with respect to their regulation and/or trafficking (Bowie 2012).

It would be challenging to directly investigate the Ca^{2+} permeability of synaptic AMPA receptors and how this property might change in different conditions. First, bi-ionic conditions as used in the present study cannot be adequately obtained with whole-cell recording and outside-out patches cannot be isolated from postsynaptic sites at AII amacrine dendrites. Second, whereas it should be possible to detect changes of *I-V* rectification of evoked EPSCs with simultaneous dual recording of synaptically coupled pairs, either pairs of rod bipolar cells and AII amacrine cells or pairs of OFF-cone bipolar cells and AII amacrine cells, *I-V* rectification and Ca^{2+} permeability might be dissociated as mentioned earlier (Bowie 2012). Recording of synaptically coupled cell pairs is also unlikely to be adequate for detailed pharmacological analysis because synaptic release from bipolar cells runs down relatively quickly. Third, measuring Ca^{2+} influx by a combination of two-photon imaging and microiontophoretic application of agonist to

dendrites of AII amacrine cells, as we did for dendritic varicosities of A17 amacrine cells (Castilho et al. 2015), can potentially provide valuable information, but cannot easily distinguish between synaptic and extrasynaptic receptors when applied to neurons in slice preparations. The technique of two-photon uncaging of neurotransmitter agonists has the highest spatial resolution, but even in this case it is difficult to ensure that only synaptic AMPA receptors are activated.

Functional consequences of diabetes-evoked changes of AMPA receptors in AII amacrine cells. In the present study we have examined diabetes-evoked changes of somatic extrasynaptic receptors. Given the lack of synaptic input from bipolar cells to the cell bodies of AII amacrines, it is not known whether these extrasynaptic receptors would encounter a glutamate concentration sufficiently high for channel opening under normal conditions. However, there is evidence for elevated levels of glutamate both in the retina of animals with experimentally induced diabetes (Lieth et al. 1998) and in the vitreous of patients with proliferative diabetic retinopathy (Ambati et al. 1997). Accumulation of glutamate in the extracellular space could be caused by reduction of glutamine synthetase in Müller cells, with consequent reduced conversion of glutamate to glutamine, by reduced oxidation of glutamate to α-ketoglutarate or by impaired uptake of glutamate by Müller cells (Li and Puro 2002; Lieth et al. 2000).

If ambient glutamate evokes channel opening, it is possible that an increased concentration of ambient glutamate in the diabetic retina could lead to reduced input resistance and thus changes in the integrative properties of AII amacrines. Another possibility is that the level of ambient glutamate primarily evokes steady-state desensitization of the extrasynaptic AMPA receptors. The reduced Ca^{2+} permeability of AMPA receptors observed here could be a mechanism for counteracting increased Ca^{2+} influx evoked by increased extracellular glutamate in the diabetic retina. In effect, the reduced Ca^{2+} permeability could be a protective mechanism rendering neurons less

susceptible to glutamate excitotoxicity. At the moment, however, we do not know if the change in Ca^{2+} permeability is caused indirectly, e.g. as a consequence of changes in extracellular glutamate, or if diabetes has a direct effect on different types of neurons and their expression of transmitter receptors.

It is not known whether the diabetes-evoked reduction of Ca^{2+} permeability for somatic extrasynaptic AMPA receptors of AII amacrines also applies to putative extrasynaptic dendritic AMPA receptors and/or synaptic AMPA receptors. The fast kinetics of Ca^{2+}-permeable AMPA receptors result in a very brief Ca^{2+} influx through these receptors, but the functional consequences of the expression of such receptors at synaptic or extrasynaptic sites in AII amacrine cells is currently unclear. Recently, a model with a preferential location of Ca^{2+}-permeable and Ca^{2+}-impermeable AMPA receptors at synaptic and perisynaptic locations of bipolar cell inputs to retinal ganglion cells was postulated (Jones et al. 2014). Varying the strength of presynaptic activation leads to differential activation of the different types of postsynaptic AMPA receptors, depending on the degree of spillout of glutamate at these synapses. If similar mechanisms are operative at the bipolar cell inputs to AII amacrines, changes in the Ca^{2+} permeability of AMPA receptors evoked by diabetes could influence the signaling and integrative properties of AII amacrine cells including the activity-driven intracellular Ca^{2+} dynamics related to regulating the strength of gap junction-mediated electrical coupling between AII amacrine cells (Kothmann et al. 2009, 2012) which is likely to be an important mechanism for post-receptoral visual adaptation (reviewed by Demb 2010).

ACKNOWLEDGEMENTS

We thank Bayer Norway for generously providing glucometers and test strips and Dr. Svein H. Mørkve for valuable advice on drug application.

GRANTS

This study was supported by the Portuguese Foundation for Science and Technology and COMPETE-FEDER (PTDC/SAU-NEU/71228/2006, to A.F.A.; SFRH/BD/30235/2006, to A.C.), the Research Council of Norway (NFR 178105, 182743, 189662, to E.H.; NFR 213776, to M.L.V.), the Western Norway Regional Health Authority (911349, to E.H.), the Odd Fellow Medical Sciences Research Fund (to E.H.), and the Asta and Mikael Aksdal Medical Sciences Research Fund (to E.H.).

AUTHOR CONTRIBUTIONS

Author contributions: A.C. and E.M. conducted electrophysiological experiments and analyzed data. A.F.A. provided ideas that contributed to the formulation of the project. E.H. and M.L.V. designed experiments, interpreted data, and supervised the project. E.H., M.L.V., and A.C. wrote the manuscript. All authors commented on and approved the final version of the manuscript.

REFERENCES

Ambati J, Chalam KV, Chawla DK, D'Angio CT, Guillet EG, Rose SJ, Vanderlinde RE, Ambati BK. Elevated γ-aminobutyric acid, glutamate, and vascular endothelial growth factor levels in the vitreous of patients with proliferative diabetic retinopathy. *Arch Ophthalmol* 115: 1161–1166, 1997.

Antonetti DA, Barber AJ, Bronson SK, Freeman WM, Gardner TW, Jefferson LS, Kester M, Kimball SR, Krady JK, LaNoue KF, Norbury CC, Quinn PG, Sandirasegarane L, Simpson IA. Diabetic retinopathy: seeing beyond glucose-induced microvascular disease. *Diabetes* 55: 2401-2411, 2006.

Bowie D. Redefining the classification of AMPA-selective ionotropic glutamate receptors. *J Physiol* 590: 49-61, 2012.

Castilho AF, Liberal JT, Baptista FI, Gaspar JM, Carvalho AL, Ambrósio AF. Elevated glucose concentration changes the content and cellular localization of AMPA receptors in the retina but not in the hippocampus. *Neurosci* 219: 23-32, 2012.

Castilho Á, Ambrósio AF, Hartveit E, Veruki ML. Disruption of a neural microcircuit in the rod pathway of the mammalian retina by diabetes mellitus. *J Neurosci* 35: 5422-5433.

Chávez AE, Singer JH, Diamond JS. Fast neurotransmitter release triggered by Ca influx through AMPA-type glutamate receptors. *Nature* 443: 705-708, 2006.

Cull-Candy S, Kelly L, Farrant M. Regulation of Ca^{2+}-permeable AMPA receptors: synaptic plasticity and beyond. *Curr Op Neurobiol* 16: 288-297, 2006.

548 **Demb JB.** Retina: microcircuits for daylight, twilight, and starlight. In: *Handbook of Brain*
549 *Microcircuits*, edited by Shepherd GM and Grillner S. New York, NY: Oxford University
550 Press, 2010, p. 193-199.
551
552 **Gardner TW, Abcouwer SF, Barber AJ, Jackson GR.** An integrated approach to diabetic
553 retinopathy research. *Arch Ophthalmol* 129: 230-235, 2011.
554
555 **Ghosh KK, Haverkamp S, Wässle H.** Glutamate receptors in the rod pathway of the
556 mammalian retina. *J Neurosci* 21: 8636-8647, 2001.
557
558 **Gowda K, Zinnanti WJ, LaNoue KF.** The influence of diabetes on glutamate metabolism
559 in retinas. *J Neurochem* 117: 309-320, 2011.
560
561 **Greger IH, Esteban JA.** AMPA receptor biogenesis and trafficking. *Curr Opin Neurobiol* 17:
562 289-297, 2007.
563
564 **Hartveit E.** Membrane currents evoked by ionotropic glutamate receptor agonists in rod
565 bipolar cells in the rat retinal slice preparation. *J Neurophysiol* 76: 401-422, 1996.
566
567 **Higley MJ, Sabatini BL.** Calcium signaling in dendritic spines. *Cold Spring Harb Perspect*
568 *Biol* 4:a005686, 2012.
569
570 **Iino M, Ozawa S, Tsuzuki K.** Permeation of calcium through excitatory amino acid
571 receptor channels in cultured rat hippocampal neurones. *J Physiol* 424: 151-165, 1990.
572
573 **Jonas P, Sakmann B.** Glutamate receptor channels in isolated patches from CA1 and CA3
574 pyramidal cells of rat hippocampal slices. *J Physiol* 455: 143-171, 1992.

Jones RS, Pedisich M, Carroll RC, Nawy S. Spatial organization of AMPAR subtypes in ON RGCs. *J Neurosci* 34: 656-661, 2014.

Kamboj SK, Swanson GT, Cull-Candy SG. Intracellular spermine confers rectification on calcium-permeable AMPA and kainate receptors *J Physiol* 486: 297-303, 1995.

Koh DS, Burnashev N, Jonas P. Block of native Ca^{2+}-permeable AMPA receptors in rat brain by intracellular polyamines generates double rectification. *J Physiol* 486: 305-12, 1995.

Kolb H, Famiglietti EV. Rod and cone pathways in the inner plexiform layer of cat retina. *Science* 186: 47-49, 1974.

Kothmann WW, Massey SC, O'Brien J. Dopamine-stimulated dephosphorylation of connexin 36 mediates AII amacrine cell uncoupling. *J Neurosci* 29: 14903-14911, 2009.

Kothmann W, Trexler EB, Whitaker CM, Li W, Massey SC, O'Brien J. Nonsynaptic NMDA receptors mediate activity-dependent plasticity of gap junctional coupling in the AII amacrine cell network. *J Neurosci* 32: 6747-6759, 2012.

Lenzen S. The mechanisms of alloxan- and streptozotocin-induced diabetes. *Diabetologia* 51: 216-226, 2008.

Li Q, Puro DG. Diabetes-induced dysfunction of the glutamate transporter in retinal Müller cells. *Invest Ophthalmol Vis Sci* 43: 3109–3116, 2002.

Li W, Trexler EB, Massey SC. Glutamate receptors at rod bipolar ribbon synapses in the

602 rabbit retina. *J Comp Neurol* 448: 230-249, 2002.
603
604 **Lieth E, Barber AJ, Xu B, Dice C, Ratz MJ, Tanase D, Strother JM.** Glial reactivity and
605 impaired glutamate metabolism in short-term experimental diabetic retinopathy. Penn
606 State Retina Research Group. *Diabetes* 47: 815–820, 1998.
607
608 **Lieth E, LaNoue KF, Antonetti DA, Ratz M.** Diabetes reduces glutamate oxidation and
609 glutamine synthesis in the retina. The Penn State Retina Research Group. *Exp Eye Res* 70:
610 723–730, 2000.
611
612 **McGuire BA, Stevens JK, Sterling P.** Microcircuitry of bipolar cells in cat retina. *J Neurosci*
613 4: 2920-2938, 1984.
614
615 **Mørkve SH, Veruki ML, Hartveit E.** Functional characteristics of non-NMDA-type
616 ionotropic glutamate receptor channels in AII amacrine cells in rat retina. *J Physiol* 542:
617 147-165, 2002.
618
619 **Nelson R, Kolb H.** A17: a broad-field amacrine cell in the rod system of the cat retina. *J*
620 *Neurophysiol* 54: 592-614, 1985.
621
622 **Ng Y-K, Zeng X-X, Ling E-A.** Expression of glutamate receptors and calcium-binding
623 proteins in the retina of streptozotocin-induced diabetic rats. *Brain Res* 1018: 66-72, 2004.
624
625 **Osswald IK, Galan A, Bowie D.** Light triggers expression of philanthotoxin-insensitive
626 Ca^{2+}-permeable AMPA receptors in the developing rat retina. *J Physiol* 582: 95-111, 2007.
627

Pourcho RG, Goebel DJ. A combined Golgi and autoradiographic study of (^{3}H)glycine-accumulating amacrine cells in the cat retina. *J Comp Neurol* 233: 473-480, 1985.

Qin P, Pourcho RG. AMPA-selective glutamate receptor subunits GluR2 and GluR4 in the cat retina: an immunocytochemical study. *Visual Neurosci* 16: 1105-1114, 1999.

Raviola E, Dacheux RF. Excitatory dyad synapse in rabbit retina. *Proc Natl Acad Sci USA* 84: 7324-7328, 1987.

Santiago AR, Hughes JM, Kamphuis W, Schlingemann RO, Ambrósio AF. Diabetes changes ionotropic glutamate receptor subunit expression level in the human retina. *Brain Res* 1198: 153-159, 2008.

Santiago AR, Rosa SC, Santos PF, Cristóvão AJ, Barber AJ, Ambrósio AF. Elevated glucose changes the expression of ionotropic glutamate receptor subunits and impairs calcium homeostasis in retinal neural cells. *Invest Ophthalmol Vis Sci* 47: 4130-4137, 2006.

Sassoè-Pognetto M, Grünert U, Wässle H. Glycinergic synapses in the rod pathway of the rat retina: cone bipolar cells express the α1 subunit of the glycine receptor. *J Neurosci* 14: 5131-5146, 1994.

Semkova I, Huemmeke M, Ho MS, Merkl B, Abari E, Paulsson M, Joussen AM, Plomann M. Retinal localization of the glutamate receptor GluR2 and GluR2-regulating proteins in diabetic rats. *Exp Eye Res* 90: 244-253, 2010.

Simó R, Hernández C. Neurodegeneration in the diabetic eye: new insights and therapeutic perspectives. *Trends Endocrinol Metab* 25: 23-33, 2014.

Singer JH, Diamond JS. Sustained Ca^{2+} entry elicits transient postsynaptic currents at a retinal synapse. *J Neurosci* 23: 10923-10933, 2003.

Strettoi E, Raviola E, Dacheux RF. Synaptic connections of the narrow-field, bistratified rod amacrine cell (AII) in the rabbit retina. *J Comp Neurol* 325: 152-168, 1992.

Strettoi E, Dacheux RF, Raviola E. Cone bipolar cells as interneurons in the rod pathway of the rabbit retina. *J Comp Neurol* 347: 139-149, 1994.

Traynelis SF, Wollmuth LP, McBain CJ, Menniti FS, Vance KM, Ogden KK, Hansen KB, Yuan H, Myers SJ, Dingledine R. Glutamate receptor ion channels: structure, regulation, and function. *Pharmacol Rev* 62: 405-496, 2010.

Veruki ML, Mørkve SH, Hartveit E. Functional properties of spontaneous EPSCs and non-NMDA receptors in rod amacrine (AII) cells in the rat retina. *J Physiol* 549: 759-774, 2003.

672 **FIGURE LEGENDS**

673 Fig. 1. AII amacrine cells in retinal slices: visualization, identification, isolation of
674 nucleated patches, and AMPA-evoked current. *A*: infrared differential interference
675 contrast videomicrograph of an AII amacrine cell in a retinal slice. Arrow points to cell
676 body and apical dendrite. The retinal layers are indicated by abbreviations (OPL, outer
677 plexiform layer; INL, inner nuclear layer; IPL, inner plexiform layer). *B*:
678 electrophysiological "signature" of an AII amacrine cell as observed in whole-cell voltage
679 clamp recording (holding potential -60 mV). Transient inward currents correspond to
680 unclamped action currents (escape from voltage clamp) evoked by 5 mV depolarizing
681 voltage pulses. *C*: infrared differential interference contrast videomicrograph of a
682 nucleated patch isolated from an AII amacrine cell (as in *A*). *D*: current activated in a
683 nucleated patch by application (500 ms) of AMPA (1.6 mM) from a theta tube pipette. The
684 trace is the average of four trials. Here, and in subsequent figures, the duration of drug
685 application is indicated by the horizontal bar above the current trace. Scale bar (*A*): 10 μm,
686 (*C*): 5 μm.
687
688 Fig. 2. Ca^{2+} permeability of AMPA receptor channels in nucleated patches from AII
689 amacrine cells is reduced in animals with streptozotocin-evoked diabetes. *A*: responses
690 evoked by application of 1.6 mM AMPA (400 ms) to a nucleated patch from a normal rat
691 under bi-ionic conditions ($[Ca^{2+}]_{out}$ = 30 mM, $[Cs^{+}]_{in}$ = 171 mM). Holding potential was
692 varied between -80 mV and 60 mV (20 mV steps). Each trace is the average of three trials.
693 *B*: Current-voltage (*I-V*) relationship of peak responses of nucleated patch in *A* (fitted with
694 a 3rd order polynomial function). *C*: responses evoked by application of 1.6 mM AMPA
695 (400 ms) to a nucleated patch from a rat with experimental diabetes under bi-ionic
696 conditions (same recording conditions as *A*). Each trace is the average of five trials. *D*: *I-V*
697 relationship of peak responses of nucleated patch in *C* (fitted with a 4th order polynomial
698 function). *E*: Reversal potentials of AMPA-evoked currents (here and later, bars represent

means ± SEMs) in nucleated patches from AII amacrine cells from normal animals (n = 7 patches), diabetic animals (n = 11 patches) and insulin-treated diabetic animals (n = 5 patches). Here and later, data from individual recordings are represented by circles. Here and later, the results from statistical comparisons between averages are indicated by n.s. (no significant difference; $P \geq 0.05$) or a single asterisk (statistically significant difference; $P < 0.05$).

Fig. 3. Ca^{2+} permeability of AMPA receptor channels in nucleated patches from AII amacrine cells is restored when animals with streptozotocin-evoked diabetes receive insulin treatment. *A*: responses evoked by application of 1.6 mM AMPA (250 ms) to a nucleated patch from a diabetic rat treated with insulin, under bi-ionic conditions ($[Ca^{2+}]_{out}$ = 30 mM, $[Cs^{+}]_{in}$ = 171 mM). Membrane potential was varied between -80 mV and 60 mV. No averaging of traces. *B*: *I-V* relationship of peak responses from nucleated patch in *A* (fitted with a 3rd order polynomial function). *C*: Ca^{2+} permeability (expressed as Ca^{2+} permeability relative to Cs^{+} permeability, P_{Ca}/P_{Cs}) of AMPA receptor channels in nucleated patches from AII amacrines in normal animals (n = 7 patches), diabetic animals (n = 11 patches) and insulin-treated diabetic animals (n = 5 patches).

Fig. 4. Inward rectification of AMPA receptor channels in nucleated patches from AII amacrine cells is reduced in animals with streptozotocin-evoked diabetes and restored when diabetic animals receive insulin treatment. *A*: responses evoked by application of 1.6 mM AMPA (350 ms) to a nucleated patch from a normal animal. Spermine (100 μM) included intracellularly (*A* - *D*). Holding potential was varied between -80 mV and 60 mV. Each trace is the average of six trials. *B*: *I-V* relationship of peak responses from nucleated patch in *A* (fitted with a 6th order polynomial function) *C*: responses evoked by application of 1.6 mM AMPA (500 ms) to a nucleated patch from a diabetic animal. Same recording conditions as in *A*. Each trace is the average of seven trials. *D*: *I-V* relationship of

726 peak responses of nucleated patch in *C* (fitted with a 4th order polynomial function). *E*:
727 rectification index of AMPA-mediated responses in nucleated patches from AII amacrines
728 in normal animals ($n = 9$ patches) and diabetic animals ($n = 10$ patches).

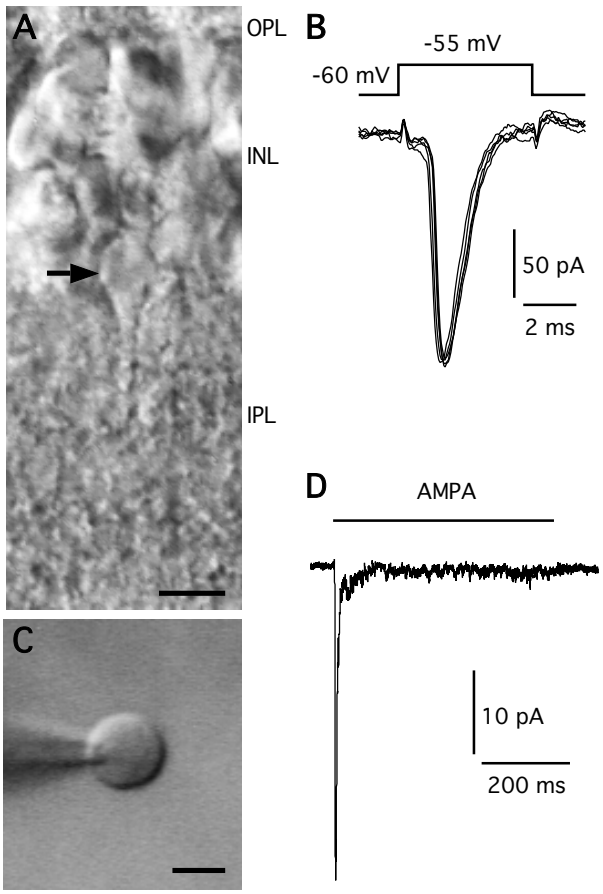

Figure 1 (Castilho et al.)

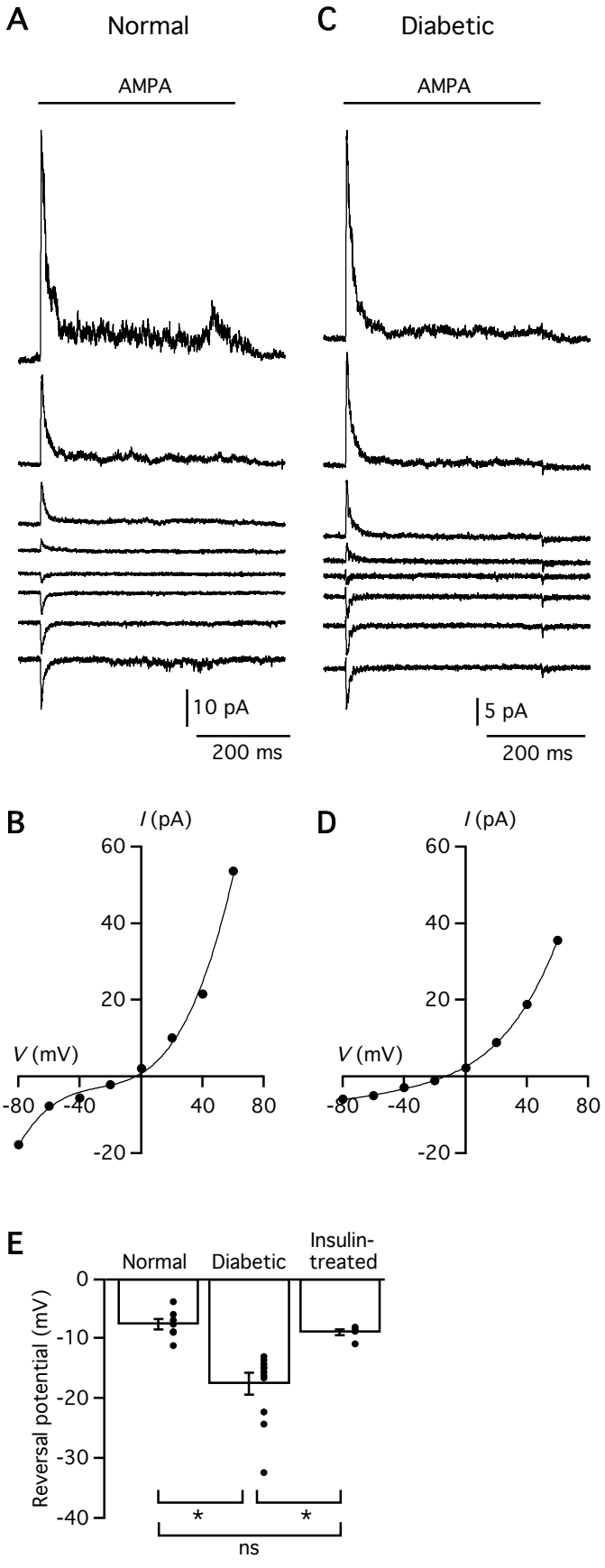

Figure 2 (Castilho et al.)

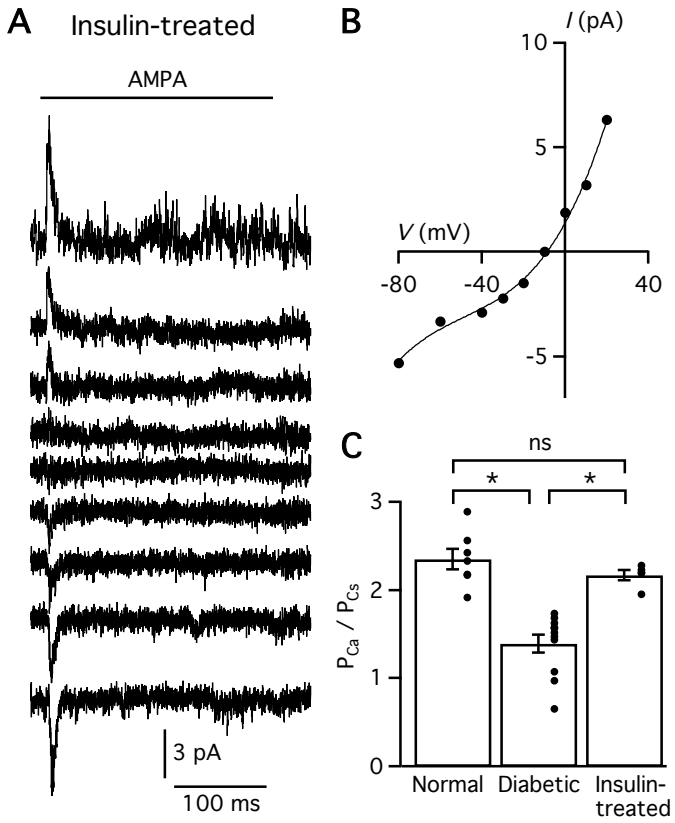

Figure 3 (Castilho et al.)

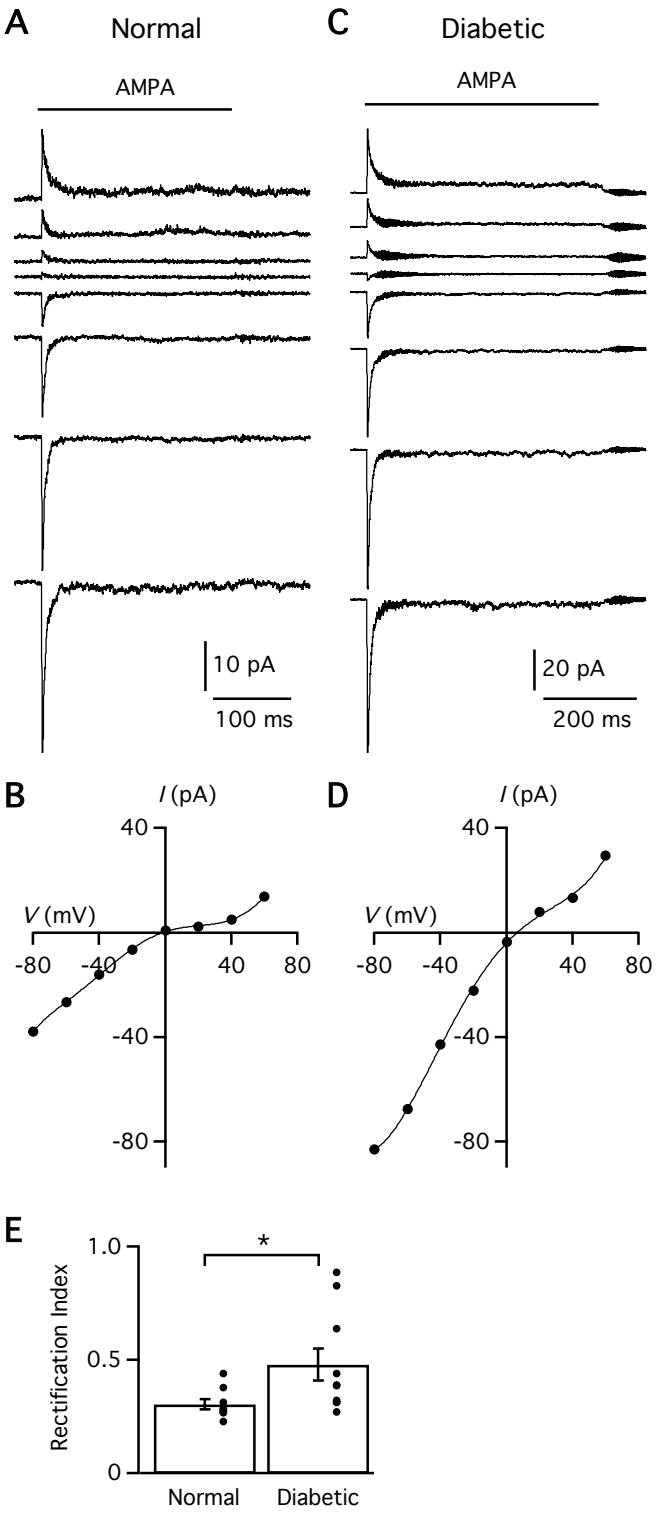

Figure 4 (Castilho et al.)